GEOPHYSICAL RESEARCH LETTERS, VOL. 24, NO. 7, PAGES 743-746, APRIL 1, 1997

Non-double-couple earthquake mechanisms at the Hengill-Grensdalur volcanic complex, southwest Iceland

B. R. Julian
U. S. Geological Survey, Menlo Park, California

A. D. Miller[1] and G. R. Foulger[1]
Dept. of Geological Sciences, University of Durham, U. K.

Abstract. The Hengill-Grensdalur area in Iceland generates frequent small non-double-couple earthquakes with explosive volumetric components. We collected high quality three-component digital recordings of 4,000 earthquakes on a purpose-designed, 32-station network in 1991, and determined focal mechanisms for 100 of the best-recorded earthquakes by inverting amplitude ratios. Many of the mechanisms are consistent, within the errors, with simultaneous shear and tensile faulting, with tensile faults parallel to the local spreading ridge, and shear faulting similar to that in the South Iceland transform-fault zone. Some events cannot be explained by this model, however, and require other processes, such as crack closing and partial compensation of tensile cracks by fluid flow.

Introduction

The Hengill-Grensdalur area, southwest Iceland (Figure 1), is a ridge-ridge-transform triple junction that contains a NNE-striking spreading segment, a tripartite volcanic complex, and extensive high-temperature geothermal resources [*Foulger and Toomey*, 1989]. It is the richest known source of non-double-couple (non-DC) earthquakes, whose mechanisms are inconsistent with simple shear faulting. *Foulger and Long* [1984] first recognized these anomalous earthquakes from the polarities of P waves recorded in 1981 on a temporary local network of 23 vertical-component seismometers. Compressive polarities were much more numerous than dilatations, indicating that the earthquakes involve volume increases. The earthquakes occur beneath the high-temperature geothermal area, and *Foulger and Long* [1984] attributed them to tensile cracking in the cooling heat source of the geothermal area. The non-DC focal mechanisms are not artifacts of wave propagation in a heterogeneous medium, as *Foulger and Julian* [1993] showed by numerically tracing rays through a three-dimensional tomographic model of the area.

Although the 1981 data rule out DC mechanisms, they have limited resolution. The P-wave polarities are consistent with narrow, band-like dilatational fields on the focal spheres, but many other patterns are possible [*Foulger*, 1988]. Here we present examples of focal mechanisms derived from polarities and amplitudes of P and S waves recorded in 1991 [*Miller*, 1996]. These results confirm that non-DC earthquakes involving volume increases are common in the Hengill-Grensdalur

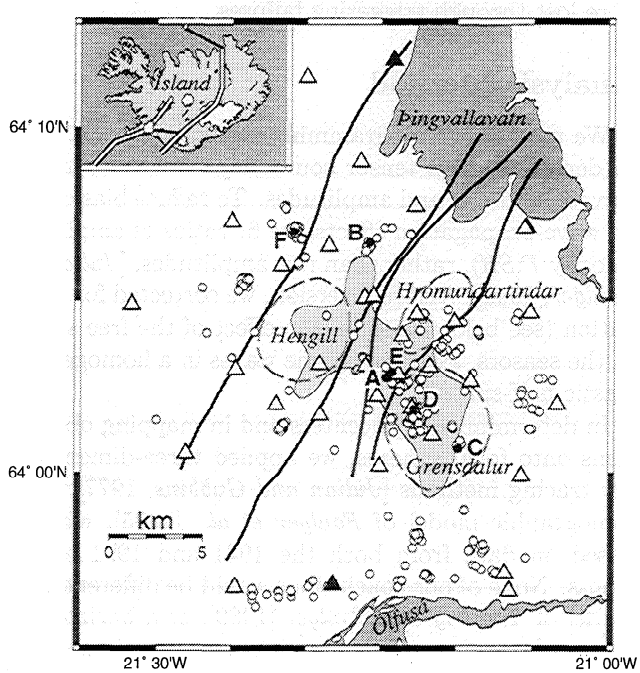

Figure 1. Map of the Hengill-Grensdalur triple junction, southwest Iceland. Open triangles: portable digital seismometers operated in August and September, 1991; filled triangles: stations of the permanent SIL digital network [*Stefánsson et al.*, 1993]. White dots: epicenters of the 391 best-located earthquakes recorded in 1991; black dots: earthquakes whose mechanisms are presented here (Table 1); dashed gray lines: outlines of volcanic centers; solid black lines: margins of the associated fissure swarms. The currently active spreading segment passes through the Hengill volcano. The transform branch is oriented east-west and lies south of the extinct Grensdalur volcano. Event B is in the Nesjavellir geothermal well field. Light gray: high-temperature geothermal area.

[1]Also at U. S. Geological Survey, Menlo Park, California.

Paper number 97GL00499.

area, resolve their focal mechanisms better, and constrain the physical processes that cause them.

Data

The aim of the 1991 experiment was to collect *P*- and *S*-phase amplitudes and waveforms, in addition to polarities, in order to resolve focal mechanisms well. We deployed 30 three-component sensors (2-Hz Mark Products L22-D) and digital recorders (REFTEK 72A-02, 100 sps/channel) in a 25×25 km pattern that gives approximately uniform coverage of the upper focal hemispheres for earthquakes in the center of the area (Figure 1). In designing the network, we mapped stations onto focal spheres by numerically tracing rays through a three-dimensional model derived from the 1981 *P* times [*Toomey and Foulger,* 1989]. Two stations of the permanent South Iceland Lowland (SIL) seismic network [*Stefánsson et al.,* 1993] also contributed data.

During the two-month recording period, Aug.–Sept. 1991, we recorded more than 100 Gbytes of data, including about 4000 earthquakes, with moment magnitudes ≤ 3.8. We recorded in continuous mode, so no data were lost through triggering failures.

Analysis Method

We used linear-programming methods [*Julian,* 1986] to derive moment-tensor source mechanisms from observed polarities and amplitudes. To reduce bias caused by wave-propagation effects, we fit ratios of amplitudes (mostly *P*:*SH*), rather than raw amplitudes, [*Julian and Foulger*, 1994]. Before inversion, we corrected for attenuation (see below) and for the effect of the free surface at the sensors, assuming plane waves in a homogeneous elastic half-space.

In determining hypocenters and in mapping observations onto focal spheres, we applied three-dimensional ray tracing methods [*Julian and Gubbins,* 1977] to the tomographic model of *Foulger et al.* [1995], which is based on data from both the 1981 and 1991 experiments. None of our conclusions would be different if the model of *Toomey and Foulger* [1989], or a horizontally averaged one-dimensional model, were used instead.

We measured polarities, amplitudes, and rise times of the initial motions of *P*, *SH*, and *SV* waves from vertical, transverse, and radial-component seismograms, obtained by numerical rotation from the field orientations. We used *SV* waves only within the "shear-wave window", where the computed incidence angle at the surface is less than 25°. Seismograms were first corrected for the acausal effects of anti-aliasing filters in the data loggers (J. Fowler, personal communication, 1993), and then low-pass filtered (3-pole Butterworth response, 5 Hz corner frequency), to reduce the effects of wave scattering and attenuation. *Julian and Foulger* [1996] show example seismograms for event D (Table 1). First-motion polarities were almost always the same on raw and filtered seismograms. Pairs of amplitudes were used in ratios only if they had similar rise times.

Table 1. Earthquakes Analyzed

Event	Date 1991	Time UTC	Depth km	M_w[a]	T	k
A	15 Aug.	09:24:25	2.85	2.1	−.72	.31
B	25 Aug.	21:26:03	4.97	2.6	.28	−.19
C	14 Sept.	07:35:03	3.83	1.9	−.20	.21
D	15 Sept.	07:41:28	4.03	1.7	.46	.27
E	21 Sept.	23:42:22	3.06	1.9	.04	.24
F	28 Sept.	04:38:25	4.53	2.3	.90	.32

[a] $M_w = {}^2/_3 \log M_0 - 6$ (M_0 in N m)

Attenuation

Attenuation by anelasticity and scattering affects compressional and shear waves differently, and multiplies observed *P*:*S* amplitude ratios by the factor

$$\exp(-\frac{\omega}{2}[Q_P^{-1}t_P - Q_S^{-1}t_S]) \,, \qquad (1)$$

where ω is angular frequency, Q_P and Q_S are the figures of merit for compressional and shear waves, and t_P and t_S are their travel times. *Menke et al.* [1995] found that at depths $\lesssim 4$ km in southwest Iceland, $Q_P^{-1} \approx 0.014$ and $Q_S^{-1} \approx 0.010$. These findings contrast with the common assumption that attenuation is caused primarily by shear anelasticity ($Q_S^{-1} \approx \frac{9}{4}Q_P^{-1}$). The values of *Menke et al.* [1995] fit our amplitude ratios better than does the assumption that shear attenuation dominates, and we used their values to correct our data. In this case compressional waves attenuate faster than shear waves but have smaller travel times, so *P*:*S* amplitude ratios are affected only weakly. In the Hengill-Grensdalur area, $t_S \approx 1.78\,t_P$, and for our data $t_P \approx 2$ s and $\omega \approx 30$ r/s, so attenuation increases *P*:*S* amplitude ratios by about 12%, and affects derived focal mechanisms only slightly.

Results

Figure 1 shows the best-determined earthquake epicenters. About 100 of these events gave well-constrained focal mechanisms, and about 76% of the *P*-wave polarities for these events are compressive. As an example, Figure 2 shows the fit to the data for event E. *Julian and Foulger* [1996] present the same information for event D. The *P* and *SH* polarities and amplitude ratios, in particular, constrain the mechanisms tightly.

Six well-constrained events illustrate the range of focal mechanisms found (Table 1). Figure 3 shows focal-sphere plots of the compressional-wave polarity fields, and Figure 4 shows the mechanisms on an orientation-independent "source-type plot" [*Hudson et al.*, 1989]. The coordinates on this plot,

$$T \stackrel{\text{def}}{=} \frac{2m_1'}{|m_3'|} \quad \text{and} \quad k \stackrel{\text{def}}{=} \frac{\text{Tr}(\mathbf{M})}{|\text{Tr}(\mathbf{M})| + 3|m_3'|} \,, \qquad (2)$$

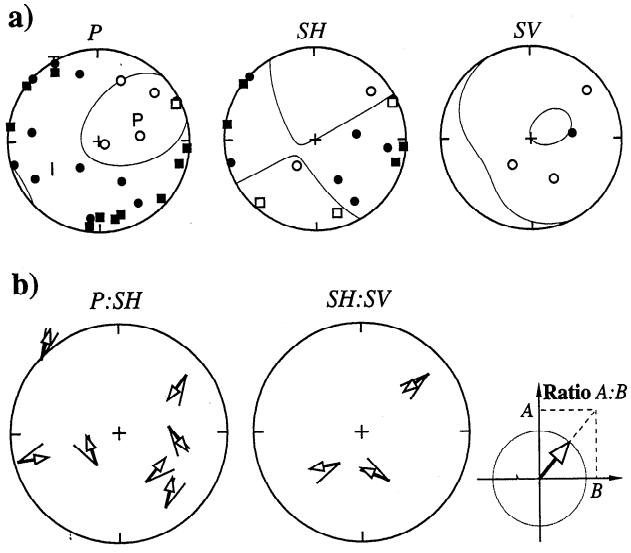

Figure 2. Derived moment tensor and observed data for event E, plotted on equal-area projections of the upper focal hemisphere. a) polarities of P, SH, and SV waves. Squares: lower-hemisphere observations plotted at antipodal points. Solid symbols indicate motion away from the source (P waves), to the right as seen from the source (SH waves) or towards the source (SV waves). Thin lines: nodal curves for derived moment tensor. b) P:SH and SH:SV amplitude ratios. Directions of arrows (of unit length) indicate the theoretical ratios (see inset). The estimated uncertainties in observed ratios are indicated by pairs of lines.

range from -1 to $+1$ and describe the deviatoric and isotropic components of the mechanism. Here **M** is the moment tensor and m_1' and m_3' are the absolutely smallest and largest deviatoric principal moments.

To assess the stability of the results, we inverted subsets of the data and studied the consistency and goodness of fit of the resulting solutions. The isotropic components of the mechanisms are generally better resolved than the deviatoric components. Eliminating 10% of the data at random typically causes variations of about 0.1 in k, and up to several times that amount in T.

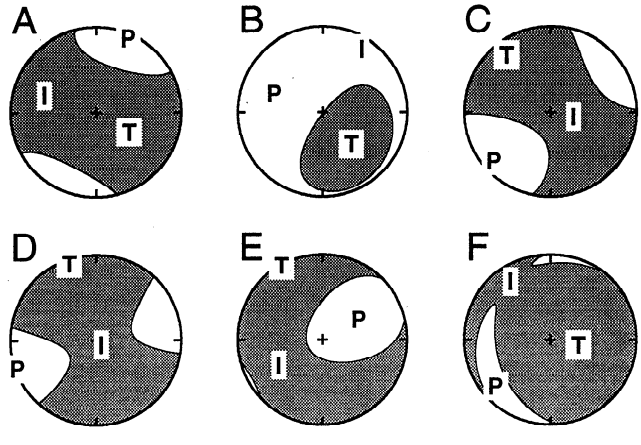

Figure 3. Focal mechanisms for the six earthquakes in Table 1, illustrating the range of results from the 1991 experiment. Shaded areas: compressive P-wave polarity fields (motion away from the source). Letters: principal-axis directions. Upper focal hemispheres in equal-area projection.

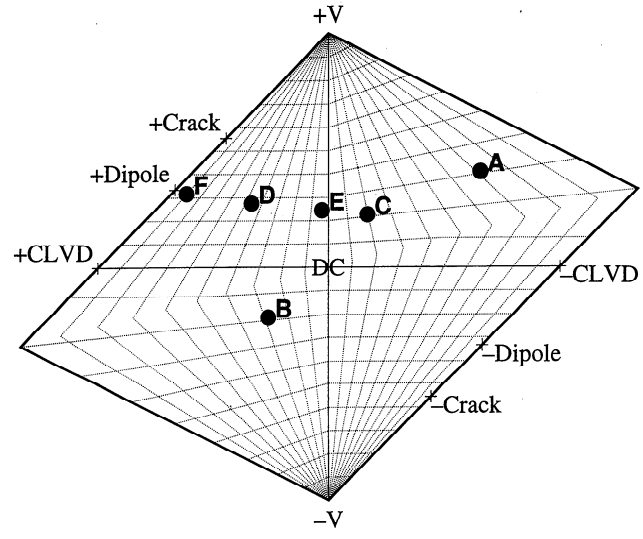

Figure 4. "Source-type plot" [*Hudson et al.*, 1989] of the mechanisms of the six earthquakes in Table 1. T ranges from -1 on the left edge to $+1$ on the right edge and describes the deviatoric component. k ranges from -1 at the bottom to $+1$ at the top and measures the isotropic (volumetric) component (Equation 2). ±DC: Locus of double couples; ±V: Isotropic volume changes; ±Dipole: Linear vector (force) dipoles; ±CLVD: Compensated linear vector dipoles; ±Crack: Opening and closing cracks.

Nearly all the well-determined mechanisms (96%) have $k > 0$, indicating volume increases, and more than 60% have $k \geq 0.2$. About 85% of the isotropic components are too large to be attributed to error. Most of these mechanisms lie near events C, D, and E in Figure 4, and are consistent, within observational uncertainty, with simultaneous shear and tensile faulting, as proposed by *Shimizu et al.* [1987]. Tensile-shear faulting mechanisms lie on the straight line connecting the DC and +Crack points on the source-type plot, if the null axis of the shear fault lies in the crack plane, and to the right of this line otherwise [*Julian et al.* 1996].

The angle between the shear and tensile faults, and hence their orientations, cannot generally be determined from the focal mechanism. For the idealized geometry described above, the crack plane is normal to the T axis if the angle between the fault planes is 45°. Under this assumption, most of our focal mechanisms indicate nearly vertical NE-SW tensile cracks, roughly parallel to the fissure swarms (Figure 1). For the shear faults, several geometrical arrangements are possible. These include right lateral motion on north-south faults and left-lateral motion on east-west faults, for both of which the P axes are horizontal, and normal motion on NE-SW striking faults, for which the P axes are vertical. The observed variation in P-axis plunges suggests that all these shear-fault geometries occur.

Some mechanisms, including events A, B, and F, are inconsistent with simultaneous shear and tensile faulting. Event B, 5 km beneath the Nesjavellir geothermal well field north of Hengill, is a rare example of an event with a significant implosive component, and probably indicates some kind of cavity collapse. This earthquake may be related to the extraction of fluid.

The mechanisms of events A and F have large CLVD components (large $|T|$), but must be considered tentative because T is poorly resolved. Physical explanations for them also are more speculative. Event A is kinematically consistent with combined shear and tensile faulting, but the geometry of the faults would have to be unusual, with P and T axes that are far from coplanar. Event F has a mechanism close to a combination of a tensile crack and an isotropic volume decrease. One possible explanation might be fluid flow into an opening crack from its surroundings.

Foulger and Long [1984] and *Foulger* [1988] interpreted their focal mechanisms in terms of tensile failure caused by thermal contraction, partially compensated by pore-fluid flow. The better-constrained mechanisms from this study show that this model is too simple. Many events are consistent with simultaneous tensile and shear faulting, but some do also require partial compensation of the volume increase of the tensile fault. *Ross et al.* [1996] report similar observations for earthquakes at The Geysers geothermal area, California, including evidence for earthquakes with volume decreases.

Conclusions

1. The occurrence of non-DC earthquakes with large explosive components in the Hengill-Grensdalur area is confirmed by high quality three-component digital data collected in 1991, analyzed using ray-tracing and amplitude-inversion techniques.

2. Most of the earthquake mechanisms are consistent with combined tensile and shear faulting, with the tensile fault vertical and striking roughly parallel to the spreading plate boundary.

3. Some well-resolved earthquakes have implosive mechanisms. These may involve cavity collapse or the compensation of tensile cracks by fluid flow.

Acknowledgments. The data used in this study were gathered with the support of a G. K. Gilbert fellowship from the U. S. Geological Survey and NERC grant GR9/134 and geophysical equipment loan 328/0990. Assistance by Sveinbjörn Björnsson of the University of Iceland, Ragnar Stefánsson, Steinunn Jakobsdóttir, and others in the Icelandic Meteorological Office, and Mary and Rex Allen was indispensable and greatly appreciated. ADM was supported by a Ph.D. studentship from the NERC, U. K., and GRF by the Nuffield Foundation. Any use of trade, firm, or product names and trademarks in this publication is for descriptive purposes only and does not constitute endorsement by the U. S. Government.

References

Foulger, G. R., and D. R. Toomey, Structure and evolution of the Hengill-Grensdalur volcanic complex, Iceland: Geology, geophysics, and seismic tomography, *J. Geophys. Res., 94,* 17511–17522, 1989.

Foulger, G. R., The Hengill triple junction, SW Iceland: 2. Anomalous earthquake focal mechanisms and implications for process within the geothermal reservoir and at accretionary plate boundaries, *J. Geophys. Res., 93,* 13507–13523, 1988.

Foulger, G. R., and R. E. Long, Anomalous focal mechanism solutions: evidence for tensile crack formation on an accreting plate boundary, *Nature, 310,* 43–45, 1984.

Foulger, G. R., and B. R. Julian, Non-Double-Couple Earthquakes at the Hengill-Grensdalur Volcanic Complex, Iceland: Are they Artifacts of Crustal Heterogeneity?, *Bull. Seismol. Soc. Am., 83,* 38–52, 1993.

Foulger, G. R., A. D. Miller, B. R. Julian, and J. R. Evans, Three-dimensional v_P and v_P/v_S structure of the Hengill triple junction and geothermal area, Iceland, and the repeatability of tomographic inversion, *Geophys. Res. Lett., 22,* 1309–1312, 1995.

Hudson, J. A., R. G. Pearce, and R. M. Rogers, Source type plot for inversion of the moment tensor, *J. Geophys. Res., 94,* 765–774, 1989.

Julian, B. R., Analysing seismic-source mechanisms by linear-programming methods, *Geophys. J. R. Astron. Soc., 84,* 431–443, 1986.

Julian, B. R., and G. R. Foulger, Earthquake mechanisms from linear-programming inversion of seismic-wave amplitude ratios: *Bull. Seismol. Soc. Am., 86,* 972-980, 1996.

Julian, B. R., and D. Gubbins, Three-dimensional seismic ray tracing, *J. Geophys., 43,* 95–113, 1977.

Julian, B. R., A. D. Miller, and G. R. Foulger, Non-double-couple earthquakes I. Theory, *Rev. Geophys.,* in press, 1997.

Menke, W., V. Levin, and R. Sethi, Seismic attenuation in the crust at the mid-Atlantic plate boundary in southwest Iceland, *Geophys. J. Int., 122,* 175–182, 1995.

Miller, A. D., Seismic structure and earthquake focal mechanisms of the Hengill volcanic complex, SW Iceland, Ph.D. thesis, Univ. of Durham, 280 pp., 1996.

Ross, A., G. R. Foulger, and B. R. Julian, Non-double-couple earthquake mechanisms at The Geysers geothermal area, California, *Geophys. Res. Lett., 23,* 877–880, 1996.

Shimizu, H., S, Ueki, and J. Koyama, A tensile-shear crack model for the mechanism of volcanic earthquakes, *Tectonophysics, 144,* 287-300, 1987.

Stefánsson, R., R. Bödvarsson, R. Slunga, P. Einarsson, S. Jakobsdóttir, H. Bungum, S. Gregersen, J. Havskov, J. Hjelme, and H. Korhonen, Earthquake prediction research in the south Iceland seismic zone and the SIL project, *Bull. Seismol. Soc. Am., 83,* 696–716, 1993.

Toomey, D. R., and G. R. Foulger, Application of tomographic inversion to local earthquake data from the Hengill-Grensdalur central volcano complex, Iceland, *J. Geophys. Res., 94,* 17497–17510, 1989.

B. R. Julian, U. S. Geological Survey, 345 Middlefield Rd. MS 977, Menlo Park, CA 94025.

A. D. Miller and G. R. Foulger, Dept. of Geological Sciences, University of Durham, Durham DH1 3LE, U. K.

(Received April 8, 1996; accepted February 19, 1997.)